MODELLISTICA E CALCOLO SCIENTIFICO

MODELING AND SCIENTIFIC COMPUTING

MOX-Report No. 18/2019

Algebraic dynamic multilevel method with local time-stepping (ADM-LTS) for sequentially coupled porous media flow simulation

Delpopolo Carciopolo, L.; Cusini, M.; Formaggia, L.;

Hajibeygi, H.

MOX, Dipartimento di Matematica
Politecnico di Milano, Via Bonardi 9 - 20133 Milano (Italy)

mox-dmat@polimi.it http://mox.polimi.it

Algebraic dynamic multilevel method with local time-stepping (ADM-LTS) for sequentially coupled porous media flow simulation

Ludovica Delpopolo Carciopolo[a,*], Matteo Cusini[b], Luca Formaggia[a], Hadi Hajibeygi[c]

[a] *MOX, Dipartimento di Matematica, Politecnico di Milano, Via Bonardi 9, 20133 Milano, Italy.*
[b] *Atmospheric, Earth, & Energy division, Lawrence Livermore National Laboratory, 7000 East Ave., Livermore, CA 94550-9234, United States of America.*
[c] *Department of Geoscience and Engineering, Faculty of Civil Engineering and Geosciences, Delft University of Technology, Stevinweg 1, 2628 CN, Delft, the Netherlands.*

Abstract

This paper presents an algebraic dynamic multilevel method with local time-stepping (ADM-LTS) for transport equations of sequentially coupled flow in heterogeneous porous media. The method employs an adaptive multilevel space-time grid determined on the basis of two error estimators, one in time and one in space. More precisely, at each time step, first a coarse time step on a coarsest space-grid resolution is taken. Then, based on the error estimators, the transport equation is solved by taking different time step sizes at different spatial resolutions within the computational domain. In this way, the method is able to use a fine grid resolution, both in space and in time, only at the moving saturation fronts. In order to ensure local mass conservation, two procedures are developed. First, finite-volume restriction operators and constant prolongation (interpolation) operators are developed to map the system across different space-grid resolutions. Second, the fluxes at the interfaces across two different time resolutions are approximated with an averaging scheme in time. Several numerical experiments have been performed

*Corresponding author.
Email addresses: `ludovica.delpopolo@polimi.it` (Ludovica Delpopolo Carciopolo), `cusini1@llnl.gov` (Matteo Cusini), `luca.formaggia@polimi.it` (Luca Formaggia), `H.Hajibeygi@tudelft.nl` (Hadi Hajibeygi)

to analyze the efficiency and accuracy of the proposed ADM-LTS method for both homogeneous and heterogeneous permeability field. The results show that the method provides accurate solutions, at the same time it reduces the number of fine grid-cells both in space and in time.

Keywords: Local time-stepping strategies, Conservative multirate methods, Algebraic Multilevel methods, Multiphase flow, Porous media

1. Introduction

Simulation of multiphase flow in natural porous media is challenging due to the variety of time and length scales involved in the process. In fact, geological formations extend for several hundreds of meters whereas physical and chemical phenomena which are of interest for many geoscientific applications (e.g., renewable energy and greenhouse gas storage, hydrocarbon production and geothermal energy extraction), occur at much smaller scales (cm and below). Moreover, fast process (e.g., high velocity flow in highly permeable rocks and fractures) and slow process (e.g., flow in low permeable porous rock) processes coexist, which have to be correctly represented to obtain reliable numerical simulations. Additionally, at the continuum (or Darcy) scale, porous media present highly heterogeneous properties (e.g., permeability). Thus, accurate numerical models require very high resolution grids both in space and time to capture all relevant physics. However, the size of the domains and the large number of simulations, required for uncertainty reduction [1, 2], make field scale simulations on such high resolution grids impractical.

Traditionally, the computational cost is reduced by employing upscaling methods [3] which define effective rock and fluid properties to represent the physics at a much coarser resolution. However, in presence of highly heterogeneous permeability fields and whenever a clear scale separation is not present, excessive upscaling may not give accurate results [4]. For this reason, advanced and scalable algorithms have to be developed to allow for efficient simulation on high resolution grids without having to define upscaled quantities.

Multiscale methods [5, 6, 7, 8, 9] and dynamic local grid refinement technique [10, 11] are among these advance simulation strategies. The first ones were developed to efficiently solve the elliptic (or parabolic) pressure equation on a coarser grid resolution, without losing the influence of the fine-

scale permeability distribution. The latter takes advantage of the locality of transport processes by dynamically adapting the grid resolution so to allow for accurate transport simulations even in presence of complex physics (e.g., [12, 4]). Recently, the Algebraic Dynamic Multilevel (ADM) method [13, 14] has been developed to combine the consistent multilevel mapping of the pressure field throughout different grid resolutions with an adaptive grid refinement technique. In ADM simulation the discrete governing equations on a high resolution grid (referred to as fine-scale) are obtained. Then, they are mapped and solved on a dynamically defined multilevel spatial grid system. The final solution can be provided both at the dynamic multilevel and fine-scale resolutions, through a sequence of prolongation and restriction operators.

Along with the advancements in the space-grid aspect of simulation, in order to reduce the overall simulation time, an implicit time integration scheme is usually employed which allows for much larger time step sizes (compared with the explicit alternative). Adaptive Implicit Methods (AIM) [15, 16, 17, 18, 19, 20], which are able to combine explicit and implicit integration schemes, have also been proposed in the literature. Despite the use of implicit integration, in presence of strong non-linearities, the Newton-Raphson method fails to converge for large time steps. As a consequence, several remedies have been proposed to enhance non-linear convergence [21, 22, 23]; these allow for the use of very large time steps and considerably improve simulation time. However, the excessive numerical dispersion introduced by the use of large time steps can significantly impact the accuracy of the solution, by, for example, smearing the advancing saturation front. Thus, multirate or local time-stepping (LTS) approaches are of great interest for porous media flow simulation. These methods employ different time step sizes within the domain based on the local flow characteristics. In earlier multirate methods, the fast and slow region were characterized a priori, based on the knowledge of the problem [24]. In a more recent work, a self-adjusting, recursive time-stepping strategy has been proposed [25]. The fast regions are detected using a time error estimator after a tentative global time step and then refined. In [26], an explicit adaptive conservative time integration techniques is presented, where the sizes of the local time steps are imposing by the CFL restriction. Very recently, a conservative implicit multirate method has been developed and analyzed for hyperbolic equations [27], and also applied to multiphase flow in heterogeneous porous media [28].

In this paper, an algebraic dynamic multilevel approach is combined with

a mass conservative local time-stepping strategy for the solution of the transport equation. The proposed simulation strategy (ADM-LTS) employs an adaptive multilevel grid both in space and in time. The dynamically defined grid resolution is chosen based on two error estimators, one in time and one in space. As a consequence, the method is able to use a fine grid resolution only at the location of the moving saturation fronts. In particular, the method first performs a global time step on the coarsest possible grid resolution. Then, thanks to the error estimators, a multilevel grid resolution is defined. On this new grid, the solution is recomputed with smaller time steps only in a fraction of the domain.

ADM-LTS is applied to homogeneous and heterogeneous 2D and 3D test cases. Systematic studies of the performance (i.e., accuracy and system complexity) have been conducted. Numerical test cases show that the ADM-LTS approach provides an accurate solution reducing the number of active cells both in space and in time.

The paper is organized as follows. The equations describing multiphase flow in porous media are presented in section 2 along with the fine-scale discrete systems for transport equation. The ADM-LTS method is explained in detail in section 3 whereas numerical experiments are presented in section 4. Finally, conclusions are provided in section 5.

2. Sequential implicit formulation for flow in porous media

Mass conservation for the flow of N_p incompressible phases in d-dimensional porous domain $\Omega \subset \mathbb{R}^d$ reads

$$\frac{\partial}{\partial t}\left(\phi S_\alpha\right) - \nabla \cdot \left(\boldsymbol{\lambda}_\alpha \cdot \nabla p\right) = q_\alpha \qquad \forall \alpha \in \{1, \ldots, N_p\}, \tag{1}$$

where capillary and gravitational effects are neglected. Here, $S_\alpha, \boldsymbol{\lambda}_\alpha$ and q_α are the α-phase saturation, mobility and source term. Additionally, p is the fluid pressure. The phase mobility $\boldsymbol{\lambda}_\alpha$ is $\boldsymbol{\lambda}_\alpha = \mathbf{K} k_{r\alpha}/\mu_\alpha$, where $\mathbf{K}, k_{r\alpha}$ and μ_α are rock absolute permeability, phase relative permeability, and viscosity, respectively. Remark that the constrain $\sum_{\alpha=1}^{N_p} S_\alpha = 1$ holds, which can be used to eliminate one saturation unknown. By summing all the phase balance equations [29],a global pressure equation is obtained, i.e.

$$-\nabla \cdot \left(\boldsymbol{\lambda}_t \cdot \nabla p\right) = q_t \quad \text{in } \Omega, \tag{2}$$

where $\boldsymbol{\lambda}_t = \sum_{i=1}^{N_p} \boldsymbol{\lambda}_i$ is the total mobility and $q_t = \sum_{i=1}^{N_p} q_i$ is the total source term. The total velocity,defined as $\boldsymbol{u}_t = \sum_{i=1}^{N_p} \boldsymbol{u}_i$, can be computed as

$$\boldsymbol{u}_t = -\boldsymbol{\lambda}_t \cdot \nabla p \qquad \text{in } \Omega. \tag{3}$$

Thus, the $(N_p - 1)$ saturation equations can be rewritten as

$$\frac{\partial}{\partial t}(\phi S_\alpha) + \nabla \cdot (f_\alpha \boldsymbol{u}_t) = f_\alpha q_t \qquad \forall \alpha \in \{1, \ldots, N_{p-1}\}, \tag{4}$$

where f_α is the fractional flow function $f_\alpha = \boldsymbol{\lambda}_\alpha / \boldsymbol{\lambda}_t$. Equations (2), (3) and (4) are coupled by the total velocity and the (nonlinear) phases relative permeability $k_{r\alpha}$.

Sequential implicit simulation (SIM) consists of decoupling the pressure and the transport equation and solve them implicitly in time. Given the state at a current time t^n, the solution at time t^{n+1} is found by first solving Eq. (2), freezing all saturation dependencies, i.e.,

$$\nabla \cdot \left(\boldsymbol{\lambda}_t(S_\alpha^n) \cdot \nabla p^{n+1}\right) = q_t \quad \text{in } \Omega. \tag{5}$$

Then, given the pressure field, the total velocity is computed as

$$\boldsymbol{u}_t^{n+1} = -\boldsymbol{\lambda}_t(S_\alpha^n) \cdot \nabla p^{n+1} \qquad \text{in } \Omega. \tag{6}$$

Finally the transport equations are solved, i.e.

$$\phi \frac{S_\alpha^{n+1} - S_\alpha^n}{\Delta t} + \nabla \cdot \left(f_\alpha^{n+1} \boldsymbol{u}_t^{n+1}\right) - f_\alpha^{n+1} q_t = 0 \quad \forall \alpha \in \{1, \ldots, N_{p-1}\}. \tag{7}$$

The saturation equations are non-linear functions. Thus, Eq. (7) is solved with a Newton-Raphson's method and at each Newton's iteration, a system of the form $\mathsf{J}^\nu \delta \mathsf{x}^{\nu+1} = -\mathsf{r}^\nu$ has to be solved. Here, $\delta \mathsf{x}$ is the vector of increment for α-saturation, J is the Jacobian matrix and r is the residual.

Let us now consider a two-phase system of a wetting (w) and a non wetting (nw) phase. For such a system, for cell K one can write

$$\mathsf{r}_{w_K}^{n+1} = (S_{w_K}^{n+1} - S_{w_K}^n) - \frac{1}{\phi |K|} \sum_{e_{KL} \in \mathcal{E}_K} e_{KL} F_{e_{KL}}^{n+1} \left(u_{t_{KL}}^{n+1} + q_t^{n+1}\right) = 0. \tag{8}$$

Here, $|K|$ is the volume of element K and e_{KL} is the interface area between cells K and L and $\mathcal{E}_K$ is the set of faces e of the element K. Finally, $F_{e_{KL}}^{n+1} u_t^{n+1}$ is the numerical flux computed using the first-order upwind method, i.e.,

$$F_{e_{KL}}^{n+1} = \begin{cases} \Delta t f_\alpha(S_{w_U}^{n+1}) & \text{if } u_{T_{KL}} > 0 \\ \Delta t f_\alpha(S_{w_D}^{n+1}) & \text{otherwise,} \end{cases} \tag{9}$$

where, S_U and S_D denote the upstream and downstream saturation values, respectively.

The quality of the solution of Eq. (7) is highly influenced by the resolution of the spatial and time discretization scheme. The objective of this work is the development of an algebraic dynamic multilevel method with local time-stepping (ADM-LTS) to solve efficiently and accurately Eq. (7) by employing a refined grid both in time and in space around the moving saturation front.

3. ADM-LTS method

In this section, first, the original ADM method [13] is reviewed, then, the newly proposed ADM-LTS algorithm is presented in details.

3.1. The ADM method

The ADM method is employed to reduce the computational cost associated with the solution of the linear system arising from the linearized Eq. (7).

Let us consider a domain discretized with a high resolution grid which is assumed to be fine enough to capture all relevant physics and to honour the heterogeneous distribution of the geological properties. Given this fine-scale discretization, a hierarchy of n_l nested coarse grids is constructed. Each grid is formed by $N_l = N_{lx} \times N_{ly} \times N_{lz}$ grid cells, where l is the resolution index and $l = 0$ represents the fine grid resolution.

The set of all grid cells belonging to resolution level l is called Π^l. At each time step ADM defines a multilevel grid by combining grid cells belonging to the hierarchy of grids previously defined. Given a multilevel ADM grid, let us define Ω^l as the set of grid cells belonging to all levels from 0 to l which are present in the ADM grid. Additionally, it is convenient to define the set Γ^l as $\Gamma^l = \Omega^l \cap \Pi^l$.

Given an ADM grid formed by the set of grid cells Ω^l, ADM assumes that the fine scale solution can be approximated by employing a sequence of prolongation operators, i.e.

$$\delta \mathsf{x}_{w_f} \approx \delta \mathsf{x}'_w = \hat{\mathsf{P}}^1_0 \dots \hat{\mathsf{P}}^l_{l-1} \delta \mathsf{x}_w. \tag{10}$$

Here, operator $\hat{\mathsf{P}}^i_{i-1}$ interpolates the solution at level i to the finer resolution level $(i-1)$ and $\delta \mathsf{x}^{ADM}_w$ is the ADM solution on the adaptive multilevel grid. The fine-scale Jacobian system is mapped to the ADM grid by

$$\hat{\mathsf{R}}^{l-1}_l \dots \hat{\mathsf{R}}^0_1 \mathsf{J} \hat{\mathsf{P}}^1_0 \dots \hat{\mathsf{P}}^l_{l-1} \delta \mathsf{x}^{ADM}_w = -\hat{\mathsf{R}}^{l-1}_l \dots \hat{\mathsf{R}}^0_1 \mathsf{r}_f, \tag{11}$$

where $\hat{\mathsf{R}}_i^{i-1}$ is the restriction operator and it maps the solution from resolution at level i to coarser level $(i-1)$. In order to ensure mass conservation at all level, a finite volume restriction operator is considered [6]. Thus, the entry (i,j) of a restriction operator reads

$$\hat{\mathsf{R}}_l^{l-1}(i,j) = \begin{cases} 1 & \text{if cell } i \in \Gamma^l \text{ and cell } j \in \Gamma^{l-1}, \\ \delta_{ij} & \text{otherwise.} \end{cases} \tag{12}$$

Additionally, constant interpolation is considered for saturation,

$$\hat{\mathsf{P}}_{l-1}^{l} = \left(\hat{\mathsf{R}}_l^{l-1}\right)^T. \tag{13}$$

3.2. ADM method with local time-stepping (ADM-LTS)

At each time step n, after having solved the pressure equation and after having computed the total velocity field, the transport equation is solved employing the ADM-LTS algorithm

First, Eq. (11) is solved over the whole domain on the coarsest grid resolution (l_{max}) formed by cells belonging to $\Pi^{l_{max}}$ and keeping refinement only around the wells, with time step Δt. Then, based on the coarse solution obtained, the proper ADM grid resolution is chosen according to a front-tracking criterion. Two alternative front-tracking strategies are considered in this work:

- a criterion based on the saturation difference between neighbouring cells. A cell i belonging to level l is refined whenever the saturation difference, as defined in [13], between i and one of its neighbours exceeds a user-defined tolerance ϵ_x.

- a time-dependent criterion is combined with the previous one to determine whether cells belonging to Π^0 should stay fine. Let us define $\psi_S = S^{n+1} - S^n$. A fine cell i is kept at the fine resolution only if $\psi_{S_i} > \epsilon_t$, where ϵ_t is a user-defined tolerance. A similar time-based coarsening criterion has successfully been used in the literature for channelized heterogeneous problems where stationary gradients are present [30].

Once the ADM grid resolution has been defined, the solution is recomputed for all cells belonging to $\Omega^{l_{max}-1}$ with a time step $\Delta t_{l_{max}-1} = \Delta t/\eta$ by imposing local boundary conditions as described in the following subsection.

Here η is the time refinement ratio. Then, the same operation is repeated for all resolution levels l until $l = 0$ has been reached. Thus, each resolution level l (formed by the set of grid blocks Ω^l) is solved with a time step $\Delta t_l = \Delta t_{l+1}/\eta$. For the finest level ($l = 0$) ADM-LTS only recomputes the solution, with time step $\Delta t_0 = \Delta t/\eta^{l_{max}}$, for a subset, defined Ω^0_A, of the cells belonging to Ω^0. Only fine cells for which $\psi'_S = S^{n+\Delta t_1} - S^n > \epsilon_t$ are part of the set Ω^0_A.

The method advances in time for the active cells in Ω^0_A until they reach $t = t^n + \Delta t_1$. Once they are synchronized, cells in Ω^1 advance in time. At this point, a new set of cells Ω^0_A is selected and these cells are advanced by Δt_1 performing η Δt_0 time steps. Once all cells in Ω^1 have reached time $t = t^n + \Delta t_2$ another time step Δt_2 can be performed for all cells belonging to Ω^2. This is a recursive procedure which is performed for all levels until all cells have reached time $t^{n+1} = t^n + \Delta t$.

Figure 1 illustrates a schematic overview of the ADM-LTS method where η and l_{max} are both equal to 2. Figure 2 shows an example of the ADM grid at each step and the refining area. At the global time step Δt, the solution is computed on the coarsest resolution l_{max}. At the intermediate time step the ADM grid resolution is defined and the solution is recomputed with the intermediate time step everywhere except at the coarsest region (middle figure). At the end, the method checks the errors and defines the set of active cells Ω^0_A (pink region on the right), the solution is recomputed with the smallest time step.

3.2.1. Local systems and local boundary conditions

For each resolution level l, the set of grid cells Ω^l is solved with the corresponding time step $\Delta t_l = \dfrac{\Delta t}{\eta^{(l_{max}-l)}}$. The number of active cells contained by Ω_l is N^l_A.

When solving for the cells belonging to Ω^l, the numerical flux at the interface between two cells K and L such that $K \in \Omega^l \wedge L \in \Gamma^{l+1}$ is approximated by

$$F^{n+\beta(i)}_{KL} = \frac{F^{n+\gamma(j)}_{KL}}{\eta} \tag{14}$$

where

$$\beta(i) = \frac{i}{\eta^{(l_{max}-l)}}, \quad i = \{1 \cdots \eta^{(l_{max}-l)}\} \tag{15}$$

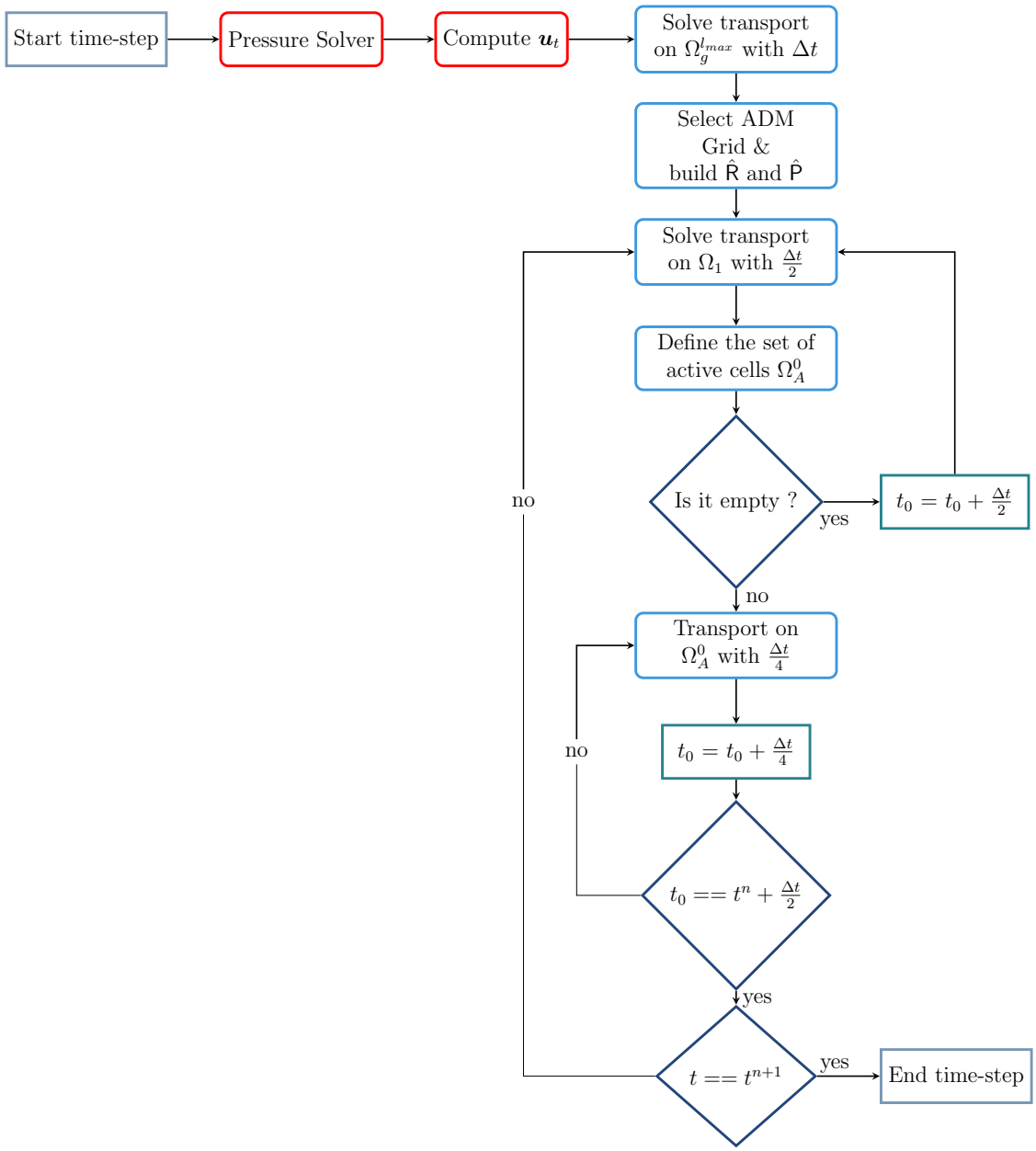

Figure 1: Schematic overview of a time step for the ADM-LTS strategy with $\eta = 2$ and $l_{max} = 2$.

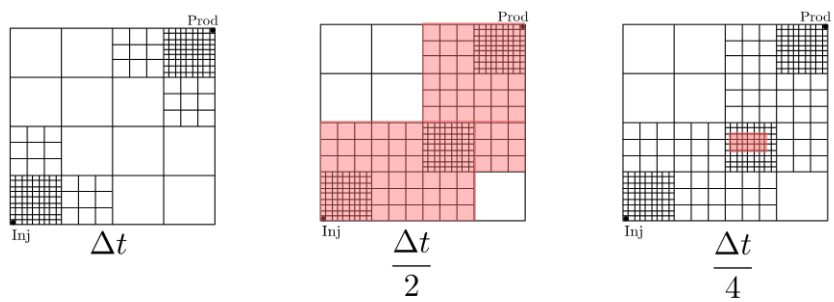

Figure 2: Example of ADM grid and active regions for the refinement time steps with $\eta = 2$ and $l_{max} = 2$.

$$\gamma(j) = \frac{j}{\eta^{(l_{max}-l-1)}}, \quad j = \{1 \cdots \eta^{(l_{max}-l-1)}\}. \tag{16}$$

Thus, Eq. (8) can be modified to account for the presence of different time levels,

$$\begin{aligned} \mathsf{r}_K^{n+\beta(i)} &= (S_{w_K}^{n+\beta(i)} - S_{w_K}^{n+\beta(i)-1}) \\ &- \frac{1}{\phi|K|} \sum_{e_{KL} \in \mathcal{E}_{KA}} e_{KL} F_{e_{KL}}^{n+\beta(i)} \left(u_{t_{KL}}^{n+\beta(i)} + q_t^{n+\beta(i)} \right) \\ &- \frac{1}{\phi|K|} \sum_{e_{KL} \in \mathcal{E}_{KL}} e_{KL} \frac{F_{e_{KL}}^{n+\gamma(j)}}{\eta} \left(u_{t_{KL}}^{n+\gamma(j)} + q_t^{n+\gamma(j)} \right). \end{aligned} \tag{17}$$

Here, $\mathcal{E}_{KA}$ is the set of interface fluxes exchanged between two cells K and L both belonging to Ω^l. Additionally, $\mathcal{E}_{KL}$ is the set of fluxes at the interface between two cells K and L where $K \in \Omega^l$ and $L \in \Gamma^{l+1}$. Note that, for $l = 0$ the residual for the active cells is the same described by equation (8) but $\mathcal{E}_{KL}$ would be the set of fluxes at the interface between Ω_A^0 and $\Omega^1 \setminus \Omega_A^0$.

Remark that, for each level l, the linear system that has to be solved has the size $N_A^l \times N_A^l$ which is significantly smaller the the full fine-scale system.

The above strategy allows for conservative multi-scale march in time and space for transport equation within the sequentially implicit simulation framework. Next, its performance is being studied for various test cases both for 2D and 3D domains.

4. Numerical results

The performance the newly developed ADM-LTS strategy is thoroughly investigated for several challenging test cases. For all cases presented, quadratic relative permeability curves are considered. Additionally, all errors are computed with respect to a reference solution, obtained by employing a high resolution discretization both in space and in time.

4.1. Test case 1: 2D homogeneous reservoir

The first test case is a 100×100 [m^2] homogeneous reservoir, with permeability of 5×10^{-15} [m^2]. A pressure-constrained wetting-phase injector well is positioned in the bottom-left corner of the domain with a pressure $p_{inj} = 10^8$ [Pa], whereas a production well is present in the top-right corner with a relative pressure of $p_{prod} = 0$ [Pa]. The phase viscosity values are $\mu_w = 10^{-3}$ [kg/m^3] and $\mu_{nw} = 10^{-2}$ [kg/m^3] for the wetting and non wetting phase, respectively. The final simulated time is 600 [days] after injection has started.

A fine-scale grid with 99×99 cells is imposed on the domain. ADM-LTS employs, a time refining ratio $\eta = 2$ and a space coarsening ratio equal to 3 in all directions. The user-defined tolerances for the coarsening and refinement criteria are $\epsilon_x = 0.07$ and $\epsilon_t = 5 \times 10^{-2}$.

Simulations are run employing three different time step sizes: 5, 10 and 20 days. Figure 3 reports the CFL values at time t = 500 days for the three different time steps for fine-scale in space simulations.

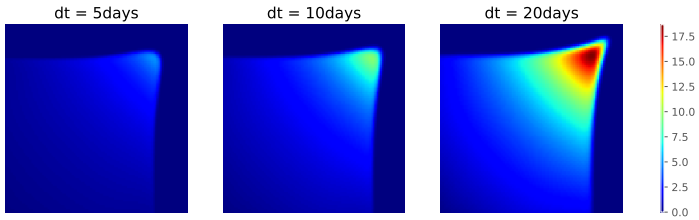

Figure 3: Test case 1 [99×99] - CFL values for different global time steps at time $t = 500$ days.

Figure 4 shows a comparison of the ADM-LTS solution with the reference solution at time t = 500 [days] using three different sizes of the global time steps.

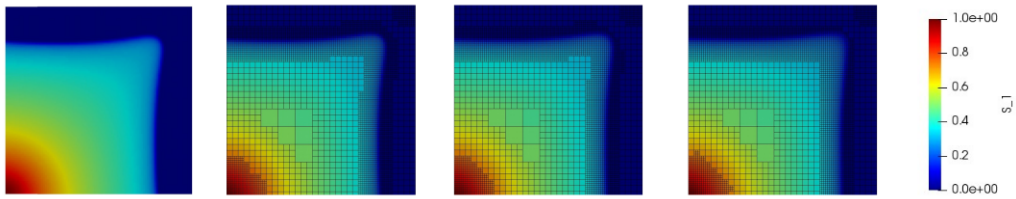

Figure 4: Test case 1 [99×99] - Reference solution (first column) and ADM-LTS solution using a global time step size: $\Delta t = 5, 10$ and 20 [days] at time t = 500 days for the second, third and fourth column, respectively.

Figure 5 reports the error for the saturation at time t = 500 days between a reference solution and the ADM method with fine time steps (first column) with the LTS approach (second column) and with the coarse time steps (third column) for the three different time steps sizes $\Delta t = 5$ (first row), $\Delta t = 10$ (second row) and $\Delta t = 20$ (third row). In all cases the AMD-LTS approach improves the errors of the coarse time step approach.

The complexity of the algorithm is shown in Fig. 6. In particular, each column represents the total amount of active cells multiplied by the number of Newton iterations involved to compute the solution, for the three approaches and for the three different global time step sizes. Note that, to obtain the solution at time t=600 [days], $120, 60$ and 30 global time steps have been performed using the three analyzed time steps. Remark that the errors obtained by employing the original ADM method with a fine time step are comparable to those obtained with ADM-LTS.

Figure 7 shows the complexity per a single global time step. For the ADM method with fine time steps, the local steps are just the small steps applied at the domain. At the end of the local steps both the ADM-LTS method and the ADM fine step method reach the same time. For the ADM-LTS method, local step 1 indicates the global step on the coarsest grid, step 2 and 5 are the intermediate time steps performed on level 0 and 1 of the ADM grid, and the other local steps are the small time steps for the active cells detected by the error estimator in time. In particular, we can notice that the intermediate time steps have almost the same complexity of the small time steps of the ADM fine method, even if the size of the time step is two times bigger with almost the same number of active cells. This is due to the improvement of the initial guess for the Newton loop. In the intermediate time steps we use as initial guess a linear combination of the solution of the previous time t^n

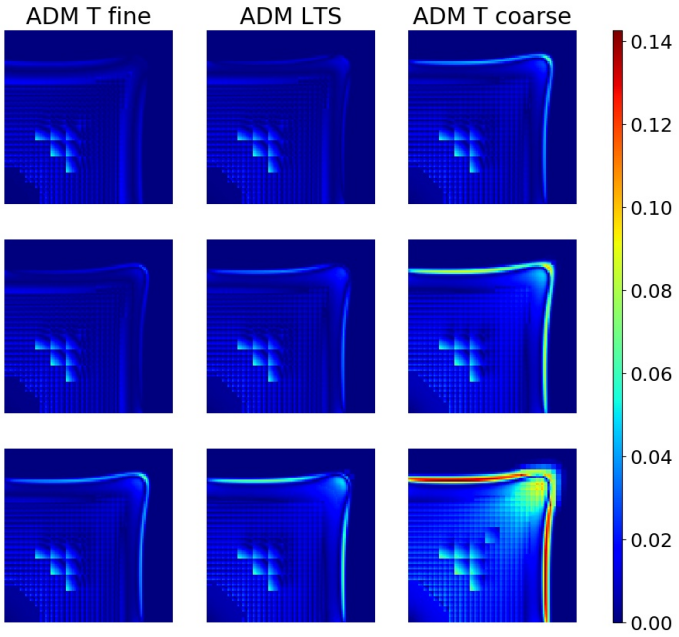

Figure 5: Test case 1 [99×99] - Saturation errors for the ADM method with fine time steps (first column), ADM-LTS method (second column) and ADM coarse time steps method (third column) for the three different global time step sizes.

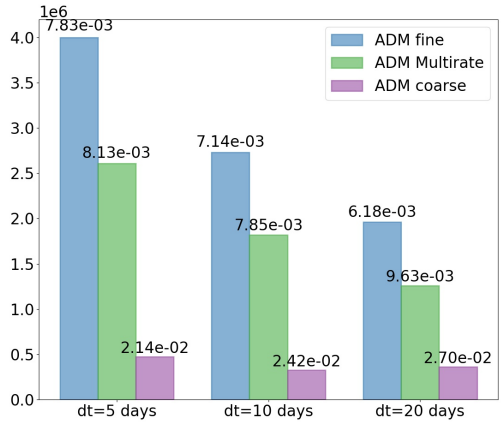

Figure 6: Test case 1 [99 × 99] - Total amount of active cells multiplied by number of Newton iterations for the three different time step sizes. On the top of each bar the mean in time of the averaged absolute difference respect to the reference solution for the saturation is displayed $E_s = \text{mean}|S(t_f) - S_{ref}(t_f)|$ where t_f is the final time 600 days.

and the solution obtained on the coarsest grid at the new global time t^{n+1}. In the small time steps is not necessary to perform this technique since a small step is used to advance in time.

The same test case is analyzed after performing a 2×2 refinement of the space fine-scale grid. In order to obtain a reasonable solution, using a global Δt equal to 20 [days], we need to compute more local time steps inside the global one, so a refining ratio equal to 4 has been taken into account.

Figure 8 reports the complexity for the entire simulation using ADM-LTS method and the ADM with fine time steps. To obtain the solution at final time t = 600 [days] with a global time step equal to 20 days, the same number of global time step are involved (30 time steps in total). Of course the number of local time step for both the LTS method and the fine time steps approach would be increased; but the ratio between active cells and total cells decreases.

Figure 9 shows the averaged number of active cells times the number of Newton iterations for each local time step within a global time step.

In Figure 10 we can see that the ADM-LTS approach reduces the errors obtained using a coarse grid in time.

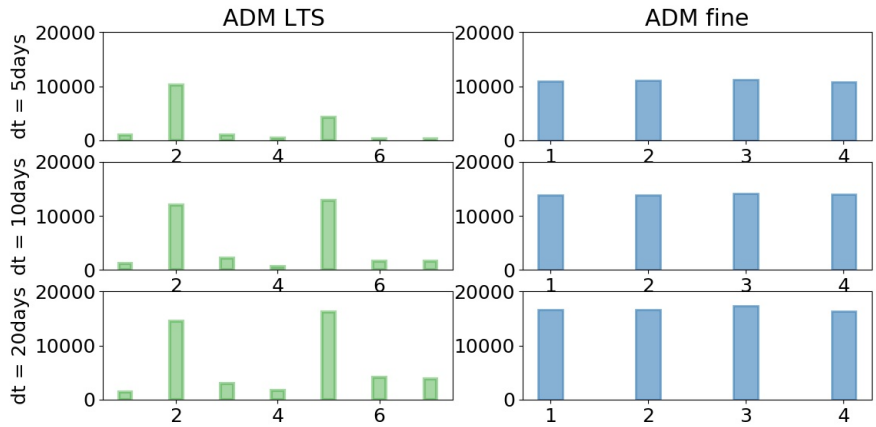

Figure 7: Test case 1 [99×99] - Computational complexity history at each local times step within a global step. The computation complexity is the number of active cells multiplied by the number of Newton iterations.

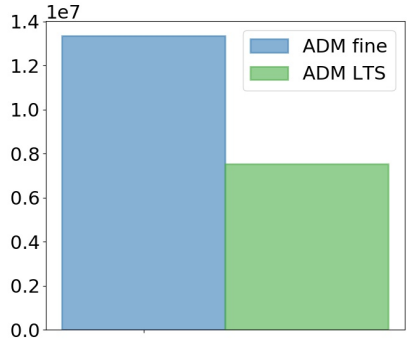

Figure 8: Test case 1 [198×198] - Total amount of active cells multiplied by number of Newton iterations for the ADM with fine time steps and the ADM LTS method.

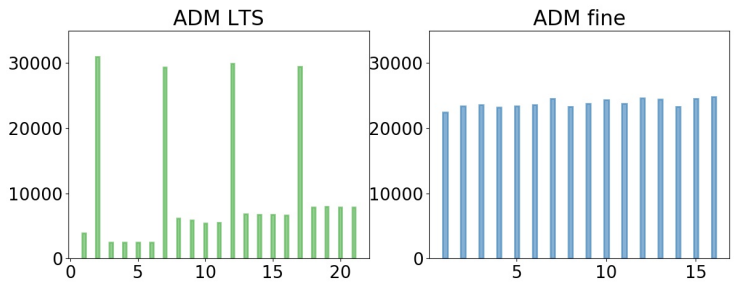

Figure 9: Test case 1 [198 × 198] - Computational complexity history at each local times step within a global step. The computation complexity is the number of active cells multiplied by the number of Newton iterations.

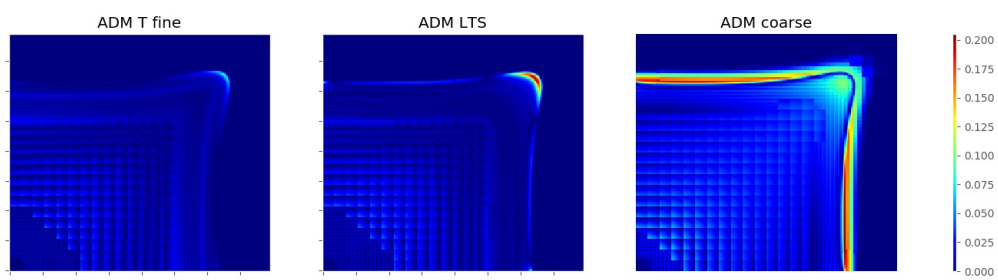

Figure 10: Test case 1 [198 × 198] - Saturation errors at time t = 540 [days] for the ADM method with fine grid in time (left), ADM-LTS method (center) and the ADM method with coarse grid in time (right).

4.2. Test case 2: 3D homogeneous reservoir

A 3D $108 \times 108 \times 108$ [m^3] homogeneous reservoir is considered in this test case. The domain is discretized, at the fine-scale, with a $54 \times 54 \times 54$ Cartesian grid for a total of 157464 cells. The physical parameters are the same of the first test case. The size of the global steps is equal to 125 days. The simulation ends after 70 global steps. The tolerances for the coarsening criteria in space and time are set to be $\epsilon_x = 0.2$ and $\epsilon_t = 5 \times 10^{-2}$.

Figure 11 reports the saturation maps at two different simulation times (on the top). For the first time the set of active cells Ω_A^0 (left, bottom) and also a section of the solution at final time t = 8750 days (right, bottom) are plotted. Note that ADM-LTS employs fine cells only around the advancing saturation front and that the active cells in time are only a fraction of them. Figure 12 shows the total complexity and the mean complexity per local time step for both the ADM-LTS method and the ADM method with fine time steps.

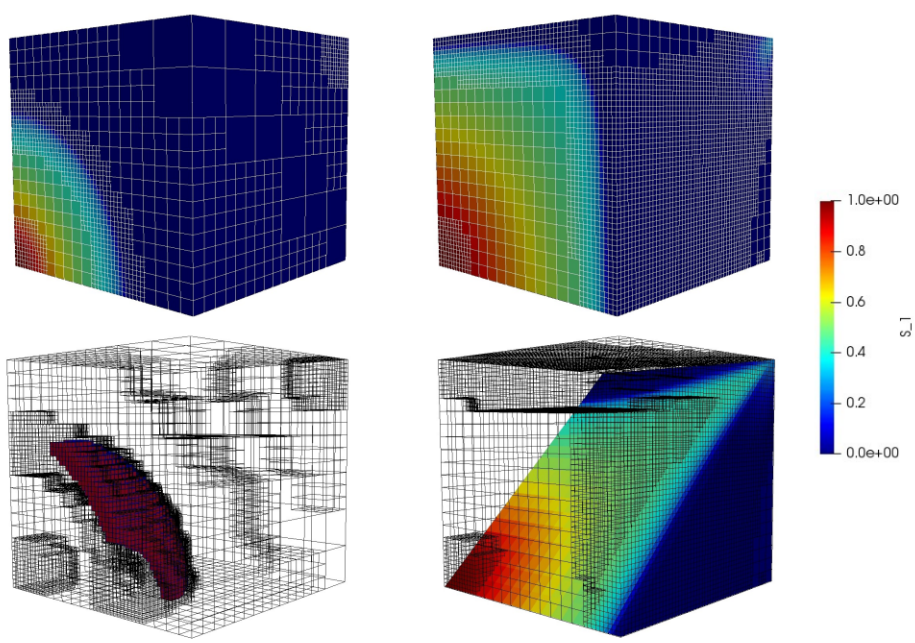

Figure 11: Test case 2 - Saturation profile (top row) at time t = 1500 days (left) and at time t = 8750 days (right). Active cells for the level $l_{ref=0}$ at time t= 1500 (bottom-left) and saturation profile inside the domain at time $t = 8750$ (bottom-right).

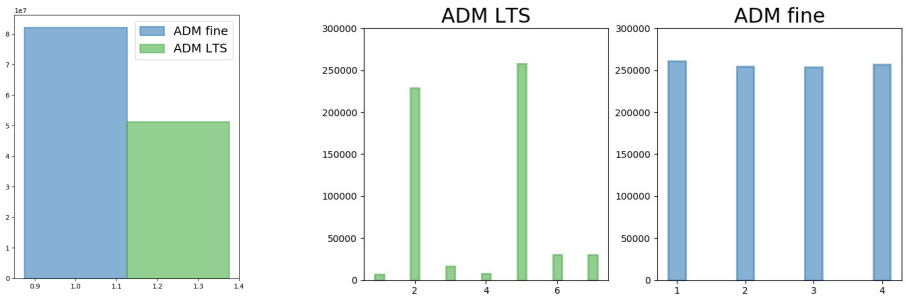

Figure 12: Test case 2 - Total amount of active cells multiplied by number of Newton iterations for the ADM with fine time steps and the ADM LTS method (left) and computational complexity history at each local times step within a global step (right).

4.3. Test case 3: 2D homogeneous reservoir with barrier

A 2D homogeneous reservoir with low permeability barriers is considered, as shown in Fig. 13. The same permeability field was presented in [30]. The domain dimensions and the physical parameters are the same of the first test case, the same 99×99 fine scale grid is imposed. The global time step is equal to 50 [days] and the simulation ends after 100 global time steps ($t = 5000$ days).

Simulations are both with the original ADM method employing a global fine time-step and with ADM-LTS. The coarsening and the time-refinement criteria tolerances are set to $\epsilon_x = 0.05$ and $\epsilon_t = 0.005$.

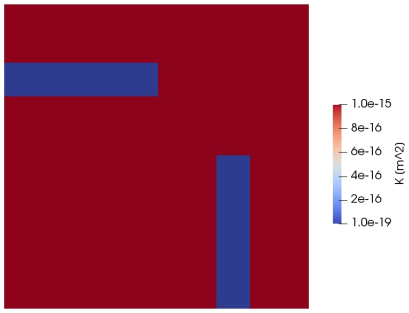

Figure 13: Test case 3 - Absolute permeability field.

Figure 14 shows a comparison of the saturation profile and the grid resolution for the two different strategies. The original ADM method with a

saturation difference-based coarsening criterion (top row) employs a lot of fine grids wherever saturation gradients are present even if they are stationary. On the other hand the newly proposed grid resolution criterion (bottom row) for the ADM-LTS approach uses fine cells only in those regions where the saturation gradient is moving, reducing the number of active cells.

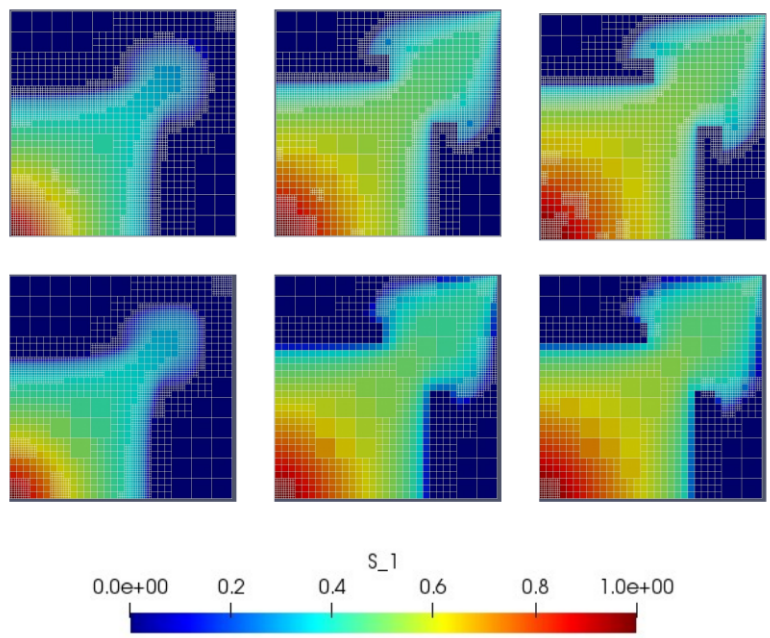

Figure 14: Test case 3 - Saturation profile and ADM grid at different time steps (columns) for ADM with coarse time steps and classical ADM grid resolution (first row) and for ADM-LTS method with the new ADM grid resolution (second row).

Figure 15 reports the evolution of the active grid cells percentage for the two different approaches (left) and the evolution of the relative saturation error in l^1-norm (right). In the early steps, we can see that the ADM fine with just the gradient resolution approach employs almost the same number of active grid cells used by the ADM-LTS method. For the ADM with fine time steps at every small local time step we solve both the flow and the transport equations, instead for the ADM-LTS approach only the transport equation is solved for the local steps. This is the reason why in the first five steps the saturation errors for the ADM-LTS approach are bigger respect to the ADM fine steps approach. Instead, in the last steps the errors increase because a lower number of fine grid cells has been used.

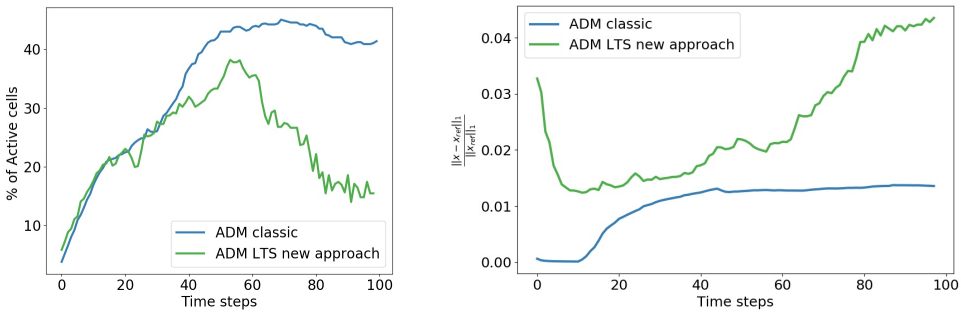

Figure 15: Test case 3 - number of active cells employed in ADM with fine grid in time and ADM-LTS simulations expressed as percentage of fine grid cells (left) and the saturation relative errors in l^1-norm for the ADM fine and ADM-LTS method (right).

Figure 16 shows the total complexity (number of active cells multiplied by the number of Newton iterations) for the ADM with fine steps and the ADM-LTS approach. Remark that the local time steps of ADM-LTS method reduce the complexity of the system compared to the classical ADM approach.

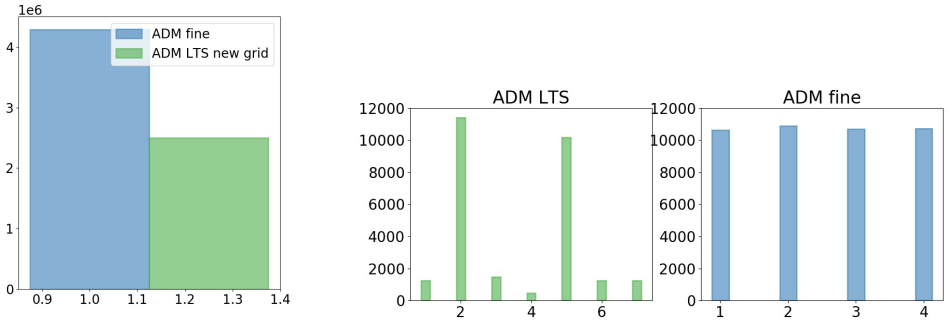

Figure 16: Test case 3 - Total amount of active cells multiplied by number of Newton iterations (left) and computational complexity history at each local times step within a global step (right) for the ADM with fine time steps approach and for the ADM-LTS method.

4.4. Test case 4: Heterogeneous reservoir (SPE10 top layer)

In this test case a heterogeneous reservoir is considered. The permeability map is the top layer of the SPE10 test case [31] and it is presented, in logarithmic scale, in Fig. 17. The size of the reservoir is 2200×600 [m^2] and

a 216×54 grid is employed at the finest level. The injector is at the top left corner and has a constrained pressure 10^7 [Pa]. A producer is, instead, located at the bottom right corner of the domain with a pressure equal to 0 [Pa]. The porosity of the reservoir ϕ is equal to 0.2. The viscosity for wetting phase is 10×10^{-5} [kg/m^3], whereas, for the non-wetting phase, is 10^{-4} [kg/m^3]. The coarsening ratio for the space grid is equal to 2 as well as the time refining ratio. The error tolerance for the time estimator is equal to 5×10^{-2}.

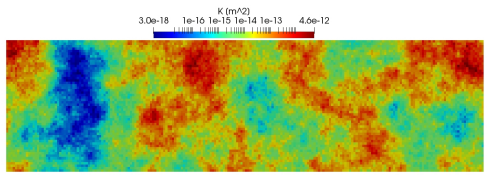

Figure 17: Test case 4 - Natural logarithm of the permeability.

Figure 18 reports the saturation map and the ADM grid for different threshold values of the ADM grid resolution criterion using the classical ADM approach with fine time steps and the ADM-LTS approach with the new grid resolution strategy. The classical approach uses, for small threshold values, a lot of fine grid cells. Relaxing the threshold parameter the method is not able to capture the fronts. Thanks to the new resolution approach, the method is able to apply the fine grid cells only where the front is moving fast (high permeability regions).

Figure 19 shows the active cells in time at the finest level $l_{ref} = 2$ for different global time steps. The method recomputes the solution with small time steps only for a few percentage of cells where the front pass high permeability regions. In fact, in the last snapshot, the saturation profile is almost evolved everywhere and so, the set of active cells, is very small.

In Figure 20 we compared the number of active cells and the saturation errors for the different simulations. Using the classical ADM approach with small values of the tolerance a lot of active grid cells are employed giving very small errors. The classical ADM approach with larger tolerance value and the ADM-LTS method are comparable in terms of active cells during all the simulation but the ADM-LTS approach gives better results in term of errors.

Figure 16 reports the complexity of the four simulations. The ADM approach with fine grid in time and small threshold values are really expensive.

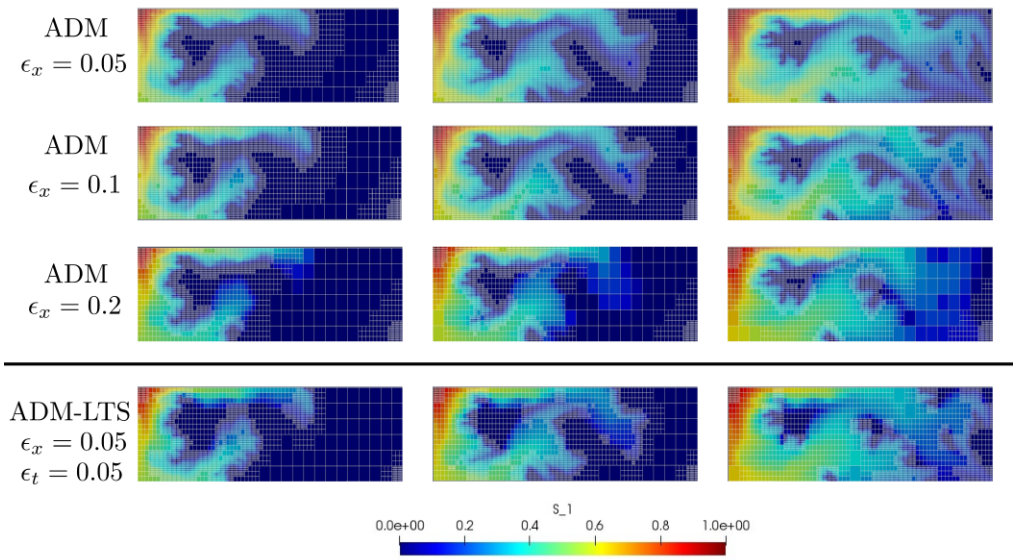

Figure 18: Test case 4 - Saturation map and ADM grid for the ADM with fine time step approach with classical grid criterion for different values of the threshold $\epsilon_x = 0.05, 0.1, 0.2$ (row 1, 2, and 3) and for the ADM-LTS method with the new grid criterion $\epsilon_x = 0.05$ and $\epsilon_t = 0.05$ (row 4) at time $t = 1200$ days (first column), $t = 15000$ days (second column) and $t = 20000$ days (third column).

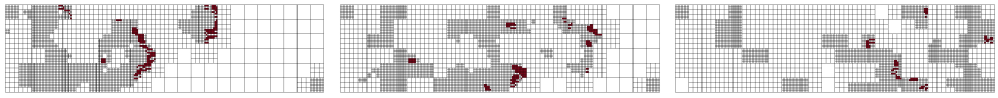

Figure 19: Test case 4 - Active cells for the refinement in time, at time $t = 1200$ days (left), $t = 15000$ days (center) and $t = 20000$ days (right).

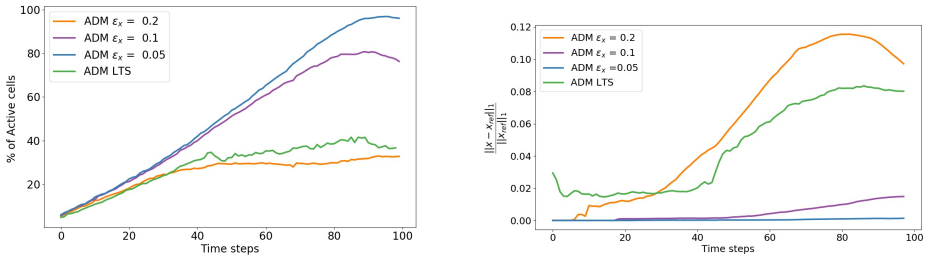

Figure 20: Test case 4 - Number of active cells expressed as percentage of fine grid cells (left) and saturation relative errors in l^1-norm (right) for the ADM with fine grid in time with different values of the threshold and for the ADM-LTS simulation.

The ADM-LTS approach is comparable to the ADM with fine time step approach and large value of ϵ_x but, as shown previously, the solution of the classic ADM, in this case, is not as accurate.

4.5. Test case 5: Heterogeneous reservoir (SPE10 bottom layer)

Permeability of SPE10 bottom layer is used for this test case, as show in Figure 22.

The global time step is equal to 10 days and the simulation ends after 50 global time steps. The input parameters for the wells and the physical properties are identical to Test Case 4.

The top 2 rows of Fig. 23 shows the saturation distribution at simulation time of 150, 250 and 350 days obtained with $\epsilon_x = 0.15$ and $\epsilon_x = 0.2$. The bottom rows, instead, show the saturation map, at the same simulations times, obtained by employing the ADM-LTS method with $\epsilon_x = 0.05$ and $\epsilon_t = 5 \times 10^{-2}$ and $\epsilon_t = 5 \times 10^{-3}$.

Figure 24 shows the active cells for the refining in time for $l_{ref} = 2$ at time 150, 250 and 350 days. As expected, for smaller value of the threshold more cells are involved in the refining step.

The history of the percentage of active cells employed by the different simulation strategies for the various tolerances is shown in Fig. 25 (left), along with the l^1 norm of the saturation error (right). For both the ADM-LTS tolerance values less active cells are involved respect to the classical ADM approach. Since a smaller number of cells is employed, the saturation errors are higher but still of the same order of magnitude.

Figure 26 reports the complexity of the four simulations for different tolerance values.

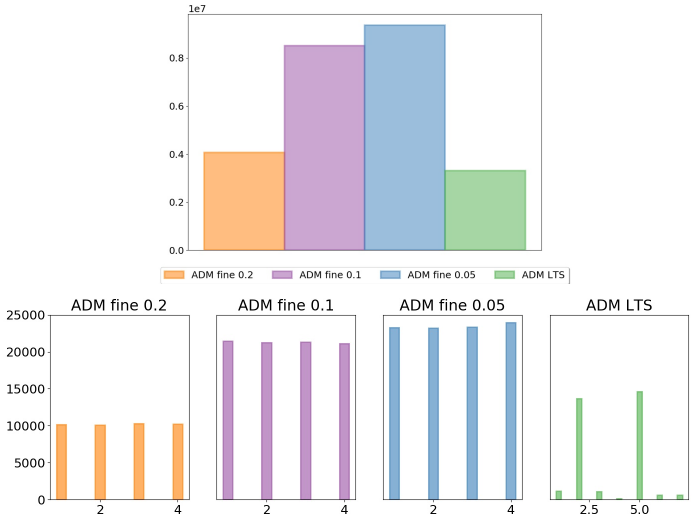

Figure 21: Test case 4 - Total amount of active cells multiplied by number of Newton iterations (top) and computational complexity history at each local times step within a global step (bottom) for the ADM approach.

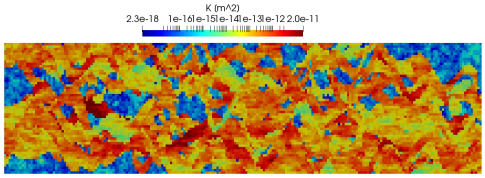

Figure 22: Test case 5 - Natural logarithm of the permeability.

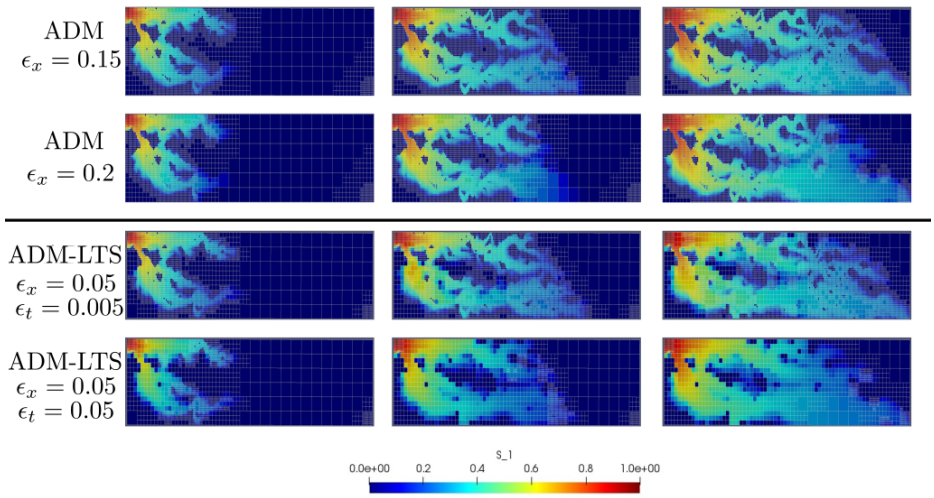

Figure 23: Test case 5 - Saturation map and ADM grid at 150, 250 and 350 days for the ADM approach with fine time steps and the ADM-LTS approach.

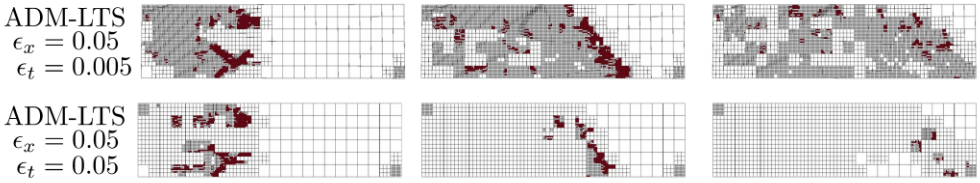

Figure 24: Test case 5 - Active cells for the refinement level $l_{ref} = 2$, at 150 (left), 250 (center) and 350 (right) days for the two threshold values.

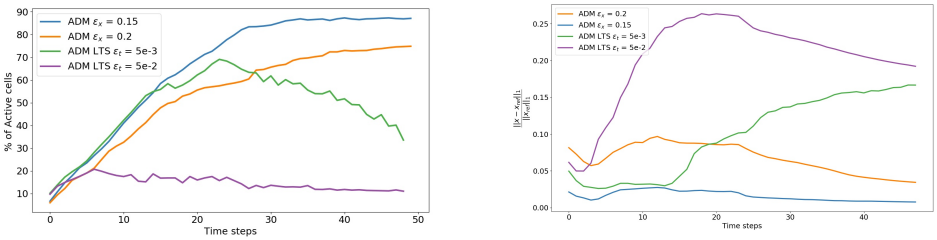

Figure 25: Test case 5 - Number of active cells expressed as percentage of fine grid cells (left) and saturation relative errors in l^1-norm (right) for the ADM with fine grid in time and for the ADM-LTS simulations.

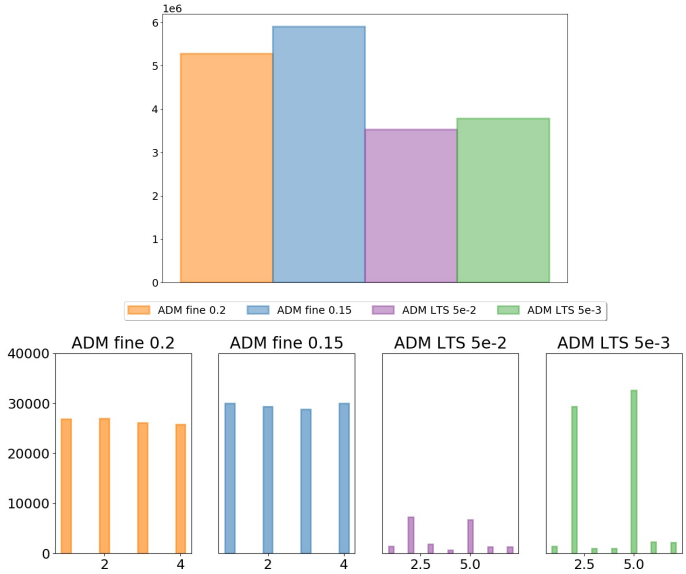

Figure 26: Test case 5 - Total amount of active cells multiplied by number of Newton iterations (top) and computational complexity history at each local times step within a global step (bottom) for the ADM approach.

4.6. Test case 6: Heterogeneous reservoirs with different layering orientations.

A 500×500 m^2 2D reservoir is considered on which a 99×99 grid is imposed. The fluid properties, the location of the wells and their constraints are the same as in the previous test cases. Five sets of permeability fields, with different layering orientation and created using sequential Gaussian simulations with spherical variogram and dimensionless correlation lengths 0.5 and 0.02 [32], are considered. Each set consists of 20 statistically identical realizations.

Figure 27 shows one realization for each set. Injection of the wetting phase, for 560 days, is simulated for each realization. Simulations are run both with the ADM-LTS method. For all runs, the spatial coarsening criterion tolerance is $\epsilon_x = 0.008$. Two different values are instead considered for the time-based criterion tolerance, ϵ_t: 5×10^{-2} and 5×10^{-3}.

Figure 28 shows a comparison, for one permeability realization of each set, of the saturation map at the end of the simulation obtained with fine-scale (time and space) simulation (top row), ADM-LTS employing a fixed refined time-step.

Figure 29 displays the active cells in time for the last refinement level of the last global time step. As expected, using bigger value of the tolerance for the time error estimator, just few cells need to be computed with small time steps, also the space grid changes and allow to use coarser grid cells.

Figure 30 represents the mean and the standard deviations of the complexity for the ADM-LTS method using the two different time-based criterion tolerances and for the solution computed with the fine grid resolution both in space and in time. Note that the y-axis scale for the two pictures are different.

Figure 31 shows the mean and the standard deviations of the saturation errors respect to the reference solution for the ADM-LTS method using the two different time-based criterion tolerances. From these studies, one can conclude that the ADM-LTS performs robust when several equiprobable realizations are considered. In other words, the error and computational complexities for all 20 realizations are not much different compared with the average values.

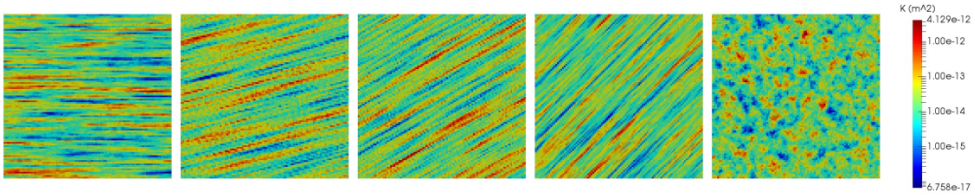

Figure 27: Test case 6 - One of the 20 realization of each of the 5 sets of permeability fields with different angles (0 deg, 15 deg, 30 deg, 45 deg and patchy from left to right).

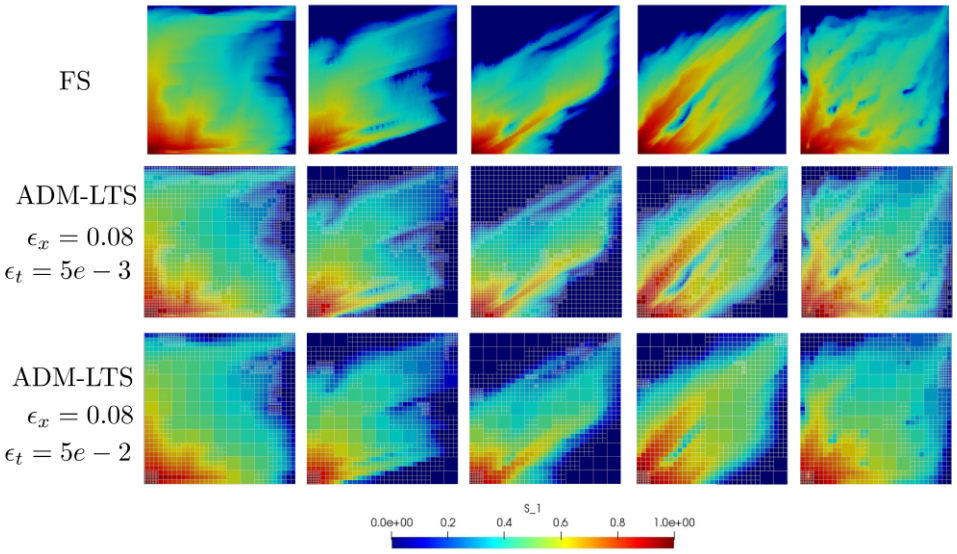

Figure 28: Test case 6 - Comparison of the saturation profile, for one realization of each set of permeability fields at time t = 560 days. Two different threshold values for the time error estimator are employed for the ADM-LTS simulation (center row and bottom row), the fine scale solution are also shown (top row).

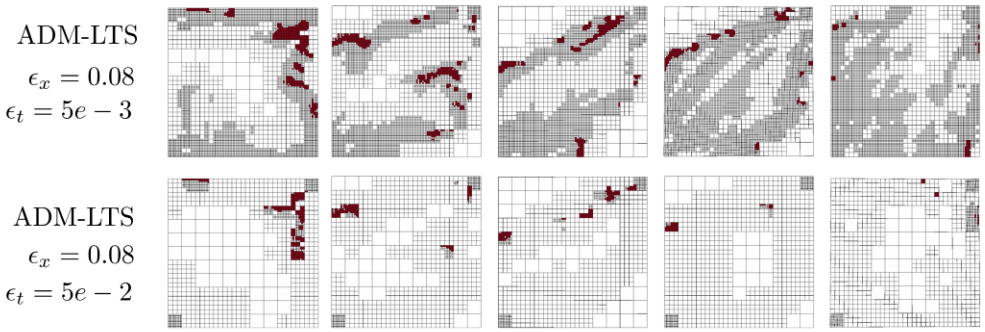

Figure 29: Test case 6 - Active calls at the last refinement level for the last global time step using two different threshold values for the error estimator in time.

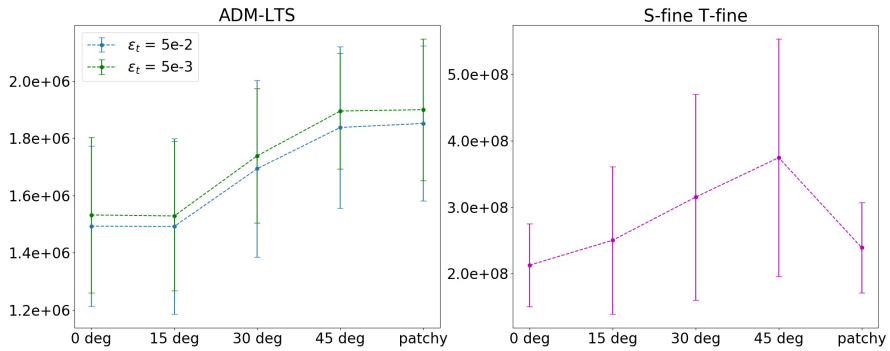

Figure 30: Test case 6 - Mean and standard deviation of complexity over 20 realization for the ADM-LTS method (left) and for the reference solution computed with fine grid resolution both in space and time (right).

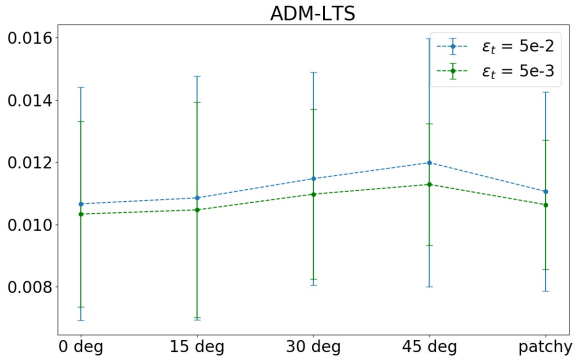

Figure 31: Test case 6: Mean and standard deviation errors of the saturation errors over 20 realization for the ADM-LTS method with different time threshold values respect to the reference solution $E_S = mean_{t=1}^{N_t}\,(mean|S_f(t) - S(t)|)$.

5. Conclusions

In this paper, a dynamic multilevel approach with a local time-stepping strategy for the solution of the transport equation in heterogeneous porous media was presented. The ADM-LTS method enables to capture the moving fronts. Particularly, it combines, at each global time step, a dynamic multilevel grid in space with a local time-stepping strategy that is able to use small time step only where the front is moving fast. Compared with the classical ADM approach, the newly developed method allows to use more coarsening regions where the high gradients do not evolve in time. This method is a promising way to reduce the size of the system in the nonlinear loop without loss of accuracy.

Acknowledgements

This work was performed in part at Delft Advanced Reservoir Simulation (DARSim) research group, and in part under the auspices of the U.S. Department of Energy by Lawrence Livermore National Laboratory (LLNL) under Contract DE-AC52-07NA27344.

References

[1] D. R. Brouwer, J. D. Jansen, Dynamic optimization of water flooding with smart wells using optimal control theory, SPE journal 4 (2004) 391–402. doi:https://doi.org/10.2118/78278-MS.

[2] R. J. de Moraes, J. R. Rodrigues, H. Hajibeygi, J. D. Jansen, Multiscale gradient computation for flow in heterogeneous porous media, Journal of Computational Physics 336 (2017) 644 – 663. doi:https://doi.org/10.1016/j.jcp.2017.02.024.

[3] L. J. Durlofsky, Upscaling and gridding of fine scale geological models for flow simulation, 8th International Forum on Reservoir Simulation Iles Borromees, Stresa, Italy 2024 (2005) 1–59.

[4] M. Cusini, R. Gielisse, H. Groot, C. van Kruijsdijk, H. Hajibeygi, Incomplete mixing in porous media: Todd-longstaff upscaling approach versus a dynamic local grid refinement method, Computational Geosciences 23 (2) (2019) 373–397. doi:10.1007/s10596-018-9802-0.

[5] T. Y. Hou, X.-H. Wu, A multiscale finite element method for elliptic problems in composite materials and porous media, Journal of computational physics 134 (1) (1997) 169–189.

[6] P. Jenny, S. Lee, H. Tchelepi, Multi-scale finite-volume method for elliptic problems in subsurface flow simulation, Journal of Computational Physics 187 (1) (2003) 47 – 67.

[7] H. Hajibeygi, G. Bonfigli, M. A. Hesse, P. Jenny, Iterative multiscale finite-volume method, Journal of Computational Physics 227 (19) (2008) 8604 – 8621.

[8] H. Zhou, H. A. Tchelepi, et al., Two-stage algebraic multiscale linear solver for highly heterogeneous reservoir models, SPE Journal 17 (02) (2012) 523–539.

[9] O. Myner, K.-A. Lie, A multiscale restriction-smoothed basis method for high contrast porous media represented on unstructured grids, Journal of Computational Physics 304 (2016) 46 – 71. doi:https://doi.org/10.1016/j.jcp.2015.10.010.

[10] M. J. Berger, J. Oliger, Adaptive mesh refinement for hyperbolic partial differential equations, Journal of Computational Physics 53 (3) (1984) 484 – 512. doi:https://doi.org/10.1016/0021-9991(84)90073-1.
URL http://www.sciencedirect.com/science/article/pii/0021999184900731

[11] B. Faigle, R. Helmig, I. Aavatsmark, B. Flemisch, Efficient multiphysics modelling with adaptive grid refinement using a mpfa method, Computational Geosciences 18 (5) (2014) 625–636. doi:10.1007/s10596-014-9407-1.
URL https://doi.org/10.1007/s10596-014-9407-1

[12] D. W. Van Batenburg, A. De Zwart, P. M. Boerrigter, M. Bosch, J. C. Vink, Application of dynamic gridding techniques to ior/eor processes, in: IOR 2011-16th European Symposium on Improved Oil Recovery, 2011.

[13] M. Cusini, C. van Kruijsdijk, H. Hajibeygi, Algebraic dynamic multilevel (adm) method for fully implicit simulations of multiphase flow in porous media, Journal of Computational Physics 314 (2016) 60 – 79. doi:https://doi.org/10.1016/j.jcp.2016.03.007.

[14] M. Cusini, B. Fryer, C. van Kruijsdijk, H. Hajibeygi, Algebraic dynamic multilevel method for compositional flow in heterogeneous porous media, Journal of Computational Physics 354 (2018) 593 – 612. doi:https://doi.org/10.1016/j.jcp.2017.10.052.

[15] G. W. Thomas, D. H. Thurnau, Reservoir simulation using an adaptive implicit method, Society of Petroleum Engineers Journal 23 (05) (1983) 759–768. doi:10.2118/10120-PA.

[16] D. A. Collins, L. X. Nghiem, Y.-K. Li, J. E. Grabonstotter, An efficient approach to adaptive- implicit compositional simulation with an equation of state, SPE Reservoir Engineering 7 (02) (1992) 259–264. doi:10.2118/15133-PA.

[17] J. Maes, A. Moncorg, H. Tchelepi, Thermal adaptive implicit method: Time step selection, Journal of Petroleum Science and Engineering 106 (2013) 34 – 45. doi:https://doi.org/10.1016/j.petrol.2013.03.019.

[18] P. Forsyth, P. Sammon, Practical considerations for adaptive implicit methods in reservoir simulation, Journal of Computational

Physics 62 (2) (1986) 265 – 281. doi:https://doi.org/10.1016/0021-9991(86)90127-0.

[19] L. S.-K. Fung, D. A. Collins, L. X. Nghiem, An adaptive-implicit switching criterion based on numerical stability analysis (includes associated paper 18727), SPE Reservoir Engineering 4 (01) (1989) 45–51. doi:10.2118/16003-PA.

[20] J. Moortgat, Adaptive implicit finite element methods for multicomponent compressible flow in heterogeneous and fractured porous media, Water Resources Research 53 (2017) 73–92. doi:10.1002/2016WR019644.

[21] P. Jenny, H. A. Tchelepi, S. H. Lee, Unconditionally convergent nonlinear solver for hyperbolic conservation laws with S-shaped flux functions, Journal of Computational Physics 228 (20) (2009) 7497 – 7512.

[22] R. Younis, H. A. Tchelepi, K. Aziz, et al., Adaptively localized continuation-newton method–nonlinear solvers that converge all the time, SPE Journal 15 (02) (2010) 526–544.

[23] F. P. Hamon, B. T. Mallison, H. A. Tchelepi, Implicit hybrid upwinding for two-phase flow in heterogeneous porous media with buoyancy and capillarity, Computer Methods in Applied Mechanics and Engineering 331 (2018) 701 – 727. doi:https://doi.org/10.1016/j.cma.2017.10.008. URL http://www.sciencedirect.com/science/article/pii/S0045782517306771

[24] J. Andrus, Numerical solution of systems of ordinary differential equations separated into subsystems, SIAM Journal of Numerical Analysis 16 (1979) 605–611.

[25] V. Savcenco, W. Hundsdorfer, J. Verwer, A multirate time stepping strategy for stiff ordinary differential equations, BIT Numerical Mathematics 47 (2007) 137–155.

[26] P. Jenny, Time adaptive conservative finite volume method, submitted.

[27] L. Delpopolo Carciopolo, L. Bonaventura, A. Scotti, L. Formaggia, A conservative implicit multirate method for hyperbolic problems, Computational Geosciencesdoi:https://doi.org/10.1007/s10596-018-9764-2.

[28] L. Delpopolo Carciopolo, L. Formaggia, S. Anna, H. Hajibeygi, Conservative multirate multiscale simulation of multiphase flow in heterogeneous porous media.

[29] R. Helmig, Multiphase Flow and Transport Processes in the Subsurface: A Contribution to the Modeling of Hydrosystems, Environmental engineering, Springer, 1997.

[30] M. Cusini, H. Hajibeygi, Algebraic dynamic multilevel (adm) method for simulations of multiphase flow with an adaptive saturation interpolator, in: ECMOR XVI-16th European Conference on the Mathematics of Oil Recovery, 2018.

[31] M. Christie, M. Blunt, Tenth SPE comparative solution project: A comparison of upscaling techniques, SPE Reservoir Simulation Symposium 11-14 February, 2001.

[32] N. Remy, A. Boucher, J. Wu, Applied geostatistics with SGeMS: a user's guide, Cambridge University Press, 2009.

MOX Technical Reports, last issues

Dipartimento di Matematica
Politecnico di Milano, Via Bonardi 9 - 20133 Milano (Italy)

17/2019 Antonietti,P.F.; De Ponti, J.; Formaggia, L.; Scotti, A.
Preconditioning techniques for the numerical solution of flow in fractured porous media

14/2019 Antonietti, P.F.; Facciolà, C; Verani, M.
Mixed-primal Discontinuous Galerkin approximation of flows in fractured porous media on polygonal and polyhedral grids

15/2019 Brandes Costa Barbosa, Y. A.; Perotto, S.
Hierarchically reduced models for the Stokes problem in patient-specific artery segments

16/2019 Antonietti, P.F.; Houston, P.; Pennesi, G.; Suli, E.
An agglomeration-based massively parallel non-overlapping additive Schwarz preconditioner for high-order discontinuous Galerkin methods on polytopic grids

13/2019 Manzoni, A; Quarteroni, A.; Salsa, S.
A saddle point approach to an optimal boundary control problem for steady Navier-Stokes equations

12/2019 Capezza, C.; Lepore, A.; Menafoglio, A.; Palumbo, B.; Vantini, S.
Control charts for monitoring ship operating conditions and CO2 emissions based on scalar-on-function regression

11/2019 Benacchio, T.; Klein, R.
A semi-implicit compressible model for atmospheric flows with seamless access to soundproof and hydrostatic dynamics

10/2019 Abramowicz, K.; Pini, A.; Schelin, L.; Sjostedt de Luna, S.; Stamm, A.; Vantini, S.
Domain selection and family-wise error rate for functional data: a unified framework

09/2019 Antonietti, P.F.; Facciola', C.; Verani, M.
Unified analysis of Discontinuous Galerkin approximations of flows in fractured porous media on polygonal and polyhedral grids

08/2019 Prouse, G.; Stella, S.; Vergara, C.; Engelberger, S.; Trunfio, R.; Canevascini, R.; Quarteroni, A
Computational analysis of turbulent haemodynamics in radiocephalic arteriovenous fistulas with different anastomotic angles